International Journal of Nanomedicine

Dovepress
open access to scientific and medical research

Open Access Full Text Article

ORIGINAL RESEARCH

Drug Repositioning of Metformin Encapsulated in PLGA Combined with Photothermal Therapy Ameliorates Rheumatoid Arthritis

Dae Kyu Kim[1,2,*], Jun Young Park[3,*], Youn Joo Kang[4], Dongwoo Khang[2,3,5]

[1]Deparment of Biochemistry, Bowdoin College, Brunswick, ME, 04011, USA; [2]Lee Gil Ya Cancer and Diabetes Institute, Gachon University, Incheon, 21999, South Korea; [3]Department of Health Sciences and Technology, GAIHST, Gachon University, Incheon, 21999, South Korea; [4]Department of Rehabilitation Medicine, Nowon Eulji Medical Center, Eulji University School of Medicine, Seoul, 01830, South Korea; [5]Department of Physiology, School of Medicine, Gachon University, Incheon, 21999, South Korea

*These authors contributed equally to this work

Correspondence: Dongwoo Khang, Department of Physiology, School of Medicine, Gachon University, Incheon, 21999, South Korea, Tel +82 32 899 6515, Fax +82 32 899 6471, Email dkhang@gachon.ac.kr; Youn Joo Kang, Department of Rehabilitation Medicine, Nowon Eulji Medical Center, Eulji University School of Medicine, Seoul, 01830, South Korea, Tel/Fax + 82-2-970-8315, Email md52516@eulji.ac.kr

Purpose: Rheumatoid arthritis (RA) is a highly prevalent form of autoimmune disease that affects nearly 1% of the global population by causing severe cartilage damage and inflammation. Despite its prevalence, previous efforts to prevent the perpetuation of RA have been hampered by therapeutics' cytotoxicity and poor delivery to target cells. The present study exploited drug repositioning and nanotechnology to convert metformin, a widely used antidiabetic agent, into an anti-rheumatoid arthritis drug by designing poly(lactic-co-glycolic acid) (PLGA)-based spheres. Moreover, this study also explored the thermal responsiveness of the IL-22 receptor, a key regulator of Th-17, to incorporate photothermal therapy (PTT) into the nanodrug treatment.

Materials and Methods: PLGA nanoparticles were synthesized using the solvent evaporation method, and metformin and indocyanine green (ICG) were encapsulated in PLGA in a dropwise manner. The nanodrug's in vitro anti-inflammatory properties were examined in J744 and FLS via real-time PCR. PTT was induced by an 808 nm near-infrared (NIR) laser, and the anti-RA effects of the nanodrug with PTT were evaluated in DBA/1 collagen-induced arthritis (CIA) mice models. Further evaluation of anti-RA properties was carried out using flow cytometry, immunofluorescence analysis, and immunohistochemical analysis.

Results: The encapsulation of metformin into PLGA allowed the nanodrug to enter the target cells via macropinocytosis and clathrin-mediated endocytosis. Metformin-encapsulated PLGA (PLGA-MET) demonstrated promising anti-inflammatory effects by decreasing the expression of pro-inflammatory cytokines (IL-1β, IL-6, and TNF-α), increasing the expression of anti-inflammatory cytokines (IL-10 and IL-4), and promoting the polarization of M1 to M2 macrophages in J774 cells. The treatment of the nanodrug with PTT exhibited more potent anti-inflammatory effects than free metformin or PLGA-MET in CIA mice models.

Conclusion: These results demonstrated that PLGA-encapsulated metformin treatment with PTT can effectively ameliorate inflammation in a spatiotemporal manner.

Keywords: rheumatoid arthritis, drug repositioning, nanoparticles, photothermal therapy

Introduction

Rheumatoid arthritis (RA), a chronic autoimmune disease, impacts millions of individuals globally, leading to cartilage deterioration, bone damage, and severe joint pain.[1] Although the root cause of RA remains elusive, the progression of RA can best be explained as an interplay of multiple inflammatory cascades.[2,3] A major inflammatory event includes the overexpression of pro-inflammatory cytokines, such as TNF-α and IL-6, which triggers synovial inflammation and joint destruction.[4] Macrophages are the most prominent cells found in inflamed synovium, and they can be classified into two types depending on their polarization state: classically activated M1 phenotype (inflammatory) and alternatively activated M2 phenotype (anti-inflammatory). Enhanced interferon signaling in inflamed regions promotes the activation of the M1

Received: 27 September 2023
Accepted: 30 November 2023
Published: 6 December 2023

Graphical Abstract

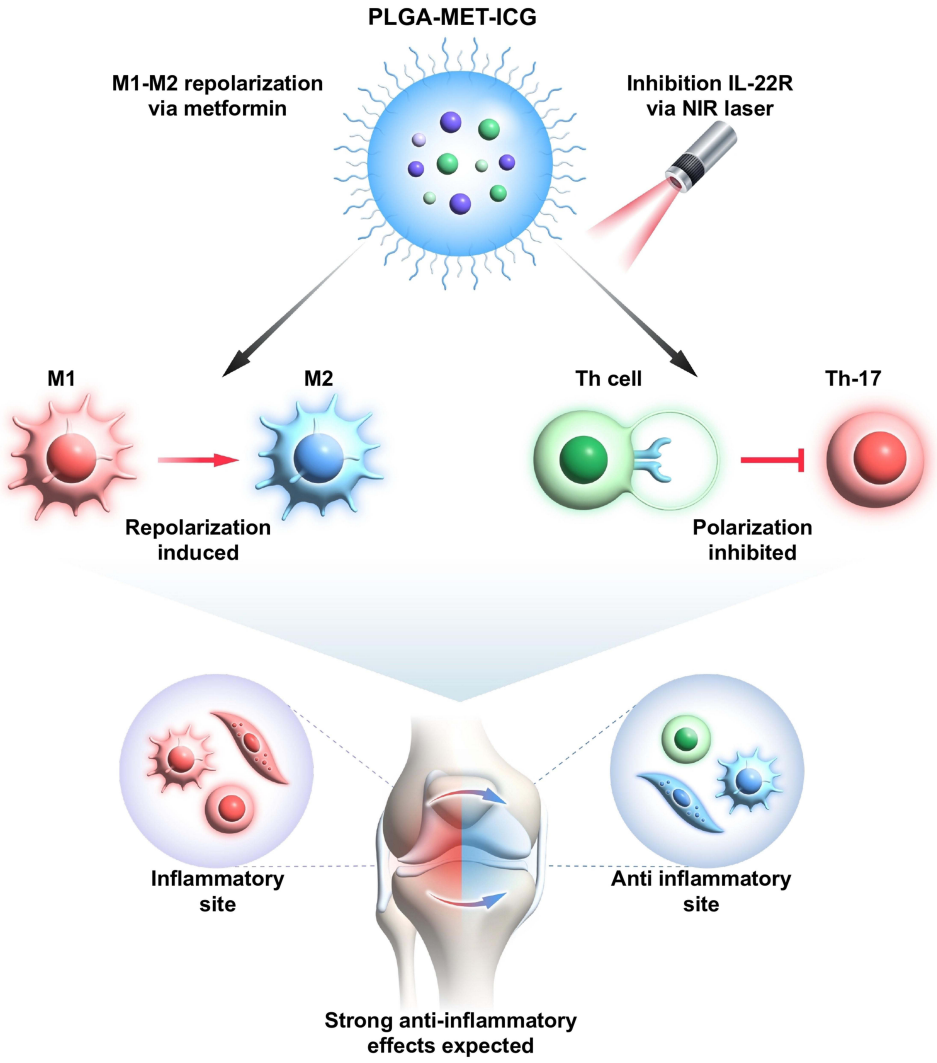

phenotype, which leads to increased production of inflammatory cytokines.[5] Contrastingly, M2 phenotype macrophages are mainly involved in anti-inflammatory responses and stimulate the production of anti-inflammatory cytokines, such as IL-4 and IL-10. Because polarization of the M1 to M2 phenotype itself is dependent on the presence of anti-inflammatory cytokines, increasing the number of M2 macrophages is important to combat RA.[6,7]

In addition to macrophages, inflammatory T cells and fibroblast-like synoviocytes (FLS) contribute to the perpetuation of rheumatoid arthritis.[8–10] Th-17, a major inflammatory T cell, is characterized by the production of IL-17 and IL-22, potent inflammatory cytokines that recruit neutrophils, monocytes, synovial fibroblasts, and macrophages. The production of these molecules results in joint inflammation and increased production of Th-17, leading to a positive feedback loop.[11] The pronounced effect of IL-17 knockout on the reduction of joint inflammation has been observed in the animal models of arthritis, suggesting the importance of Th-17 downregulation in anti-RA therapeutic strategies.[12–14] Similarly, FLS present in the inflamed synovium produce inflammatory cytokines and proteases that lead to cartilage degradation. Patients develop a unique phenotype of FLS in which the cells display increased migration into the extracellular matrix and further perpetuate inflammation.[10]

Common treatment strategies for RA include disease-modifying anti-rheumatic (DMARDs) and non-steroidal anti-inflammatory drugs (NSAIDs).[2,15] These drugs aim to ameliorate RA by either downregulating the production of inflammatory cytokines or targeting RA-inducing cells.[3] Although these agents display promising results in laboratory settings, they are often associated with gastrointestinal distress, dyspepsia, and low half-life.[16,17] Furthermore, many patients exhibit limited response to anti-RA drugs due to the emergence of drug resistance, calling for the need for novel anti-RA agents.[18] Recently, drug repositioning, which involves the process of discovering new indications of pre-existing drugs for use in a different disease, has garnered significant interest.[19] Using drug repositioning approaches, scientists have identified several FDA-approved drugs that may be promising candidates for RA treatment. Among them is metformin, an oral antidiabetic drug that is widely used to treat type II diabetes.[20,21] Besides its anti-hyperglycemic properties, metformin exhibits many anti-inflammatory effects.[18] Furthermore, many preclinical studies have demonstrated that metformin can slow the progression of RA via several mechanisms.[22–25]

Despite its promising anti-inflammatory properties, metformin-based RA treatment is associated with poor biostability under physiological conditions.[26] In our bodies, metformin exists as a highly soluble base because of its hydrophilic amine and imine groups. As a result, the half-life of metformin is approximately five hours, which is remarkably lower than the ideal half-life of oral drugs.[27,28] Moreover, because of its hydrophilicity, passive diffusion of metformin via the plasma membrane is very limited.[29] Hence, maintaining an effective level of metformin in our bodies requires repeated administration of the drug at high concentrations. However, the excessive accumulation of metformin increases the risk of gastrointestinal side effects.[29] The oral administration of metformin in patients with RA led to the development of gastrointestinal conditions, notably abdominal pain, flatulence, and diarrhea.[27] Given these undesired pharmacokinetic properties, metformin can only be suggested as a potential add-on therapy to pre-existing NSAIDs and DMARDs.

A promising approach for addressing poor pharmacokinetics is the application of nanoparticles as a drug delivery system. Due to the enhanced permeability and retention (EPR) effect, inflamed tissues and regions selectively accumulate nanoparticles, leading to targeted drug delivery.[30] Moreover, the encapsulation of drugs into nanoparticles leads to improved drug solubility, half-life, and membrane penetration.[31] The resulting compounds exhibit remarkable stability and possess a substantial drug-loading capacity, thereby enabling the potential encapsulation of a combination of therapeutic agents, such as indocyanine green (ICG), for photothermal therapy (PTT).[32,33] Upon near-infrared (NIR) irradiation, ICG acts as a photothermal agent by converting the optical energy of NIR into thermal energy.[34] The recent advances in nanotechnology have led to the development of novel drug delivery systems, such as liposomes, polymers, and magnetic nanoparticles to target RA.[35–37] Among them, poly(lactic-co-glycolic acid) (PLGA) is one of the most effective polymeric nanoparticles that has been approved by the FDA owing to its biocompatibility and biodegradability.[32] Although PLGA is widely used as a drug delivery system for RA, no study has attempted to encapsulate metformin into PLGA for anti-RA therapy. Some examples of non-PLGA encapsulated metformin compounds include metformin–loaded PEGylated solid lipid nanoparticles and metformin-loaded microbubbles.[38,39]

In the present study, metformin was encapsulated in PLGA to explore its anti-inflammatory efficacy. PLGA-Metformin (PLGA-MET) exhibited notable anti-RA effects by downregulating the production of pro-inflammatory cytokines (TNF-α, IL-1β, IL-6), upregulating the expression of anti-inflammatory cytokines (IL-10, and IL-4), and promoting the repolarization of M1 to M2 macrophages. Notably, in the process of investigating the downregulation of Th-17 precursors, it was discovered that the thermal responsiveness of the IL-22 receptor (IL-22R), in which treatment with NIR laser led to decreased expression of the IL-22 receptor. Since IL-22R is an important regulator of Th-17 cells that suppress the expression of IL-17, it was hypothesized that the application of NIR to PLGA-MET would lead to more potent anti-RA effects.[40,41] Therefore, ICG was encapsulated in PLGA-MET (PLGA-MET-ICG) to induce PTT by developing hyperthermal environments in inflamed regions upon exposure to NIR laser. As expected, PLGA-MET-ICG significantly inhibited the expression of IL-22R in J774 cells and displayed more potent anti-inflammatory effects than PLGA-MET in the arthritic mouse model. Since no previous studies have exploited the thermal responsiveness of IL-22R or the encapsulation of metformin in PLGA for RA therapy, our study is the first to demonstrate a powerful novel combination of chemotherapy, immunotherapy, and PTT for ameliorating RA.

Materials and Methods

Synthesis of Polymeric Nanoparticles

Poly lactic-co-glycolic acid (PLGA) nanoparticles were prepared using the solvent evaporation method with modifications.[42] Acid-terminated 50:50 poly($_{DL}$-lactide-co-glycolide) purchased from Durect (A17-080) was dissolved in acetone (5 mg/mL) and then added dropwise into 1% poly vinyl alcohol (Sigma, USA). The mixture was emulsified using a sonicator (Misonix S-4000) for 30s at 30% amplitude. The remaining acetone was evaporated using a rotary evaporator (Heidolph Laborota 4000), and the resulting PLGA-containing solution was centrifuged at 17,000×g for 10 minutes at 4°C.

Loading of Metformin and ICG to PLGA

Metformin hydrochloride (Sigma, USA) and indocyanine green (USP, USA) were dissolved in distilled water at a concentration of 50 μg/μL, then slowly added to 1% PVA solution before the addition of PLGA. The mixture was emulsified for 15s at 30% amplitude, followed by the dropwise addition of PLGA. The resulting solution was concentrated via centrifugation, as stated earlier, and the supernatant was collected for physicochemical analysis. The final volume of samples was 2 mL.

Physiochemical Analysis

The concentration of PLGA nanoparticles was quantified by measuring the absorbance at 700 nm using a UV-VIS spectrophotometer (Biochrom, Libra S50) according to the manufacturer's instructions. The amount of the encapsulated metformin was determined by measuring the absorbance of the supernatant at 232 nm. The previously constructed standard curves for PLGA and metformin were used to extrapolate the final concentrations of each solution. Encapsulation efficiency was calculated as the $\frac{\text{total amount of metformin} - \text{unencapsulated amount of metformin}}{\text{total amount of metformin}} \times 100$ (Table S1).[43] The hydrodynamic sizes and surface charges of the synthesized nanoparticles were measured using a Zetasizer (Anton Paar, Litesizer^{TM} 500). The synthesized nanoparticles were examined at high resolution using TEM, F30, Tecnai, USA).

Cell Culture

The J774 cell line was purchased from the American Type Culture Collection. J774 cells were cultured in Dulbecco's modified Eagle's medium (Gibco) containing 10% non-heated fetal FBS and 1% penicillin/streptomycin at 37 °C with 5% CO_2. J774 cells obtained from passages 9 to 12 were used in this experiment. T cells were isolated from 4-6-week-old male DBA/1 mice (Orient Bio, Seoul, Korea) using the EasySep^{TM} ($CD4^+$ $CD62L^+$ T cell isolation kit, StemCell) mouse T cell isolation protocol. Mouse spleen tissues were pulverized, and red blood cells were removed using RBC lysis buffer (BioLegend, United Kingdom). T cells present in minced splenocytes were isolated using magnetic beads from the EasySep^{TM} isolation kit. T cells were cultured in Roswell Park Memorial Institute 1640 medium (Gibco) containing 10% heated FBS, 1% penicillin/streptomycin, 100 mM sodium pyruvate, 50 mM 2-mercaptoethanol, 50 mg/mL gentamycin, and 100 mM NEAA at 37°C with 5% CO_2. All T cells were used within 30 h of isolation.

Cellular Uptake of PLGA Nanoparticles

J774 cells were seeded on poly-$_D$-lysine-coated coverslips at a density of 1×10^5 and incubated overnight. The cells were stimulated with either 10 ng/mL of TNF-α or 50 ng/mL of LPS for 2 h, followed by treatment with 500 ng/mL of DiO-encapsulated PLGA for 2 h. Subsequently, cells were incubated with various cellular uptake pathway inhibitors (50 μM EIPA, 200 μM GEN, and 20 μM CPZ, Sigma) for 2 h. The samples were fixed with 2% paraformaldehyde in the appropriate medium at 4 °C overnight. The cellular uptake of PLGA-DiOs by J774 cells was analyzed using confocal fluorescence microscopy EVOS M7000, Invitrogen). The endocytic pathways of the nanoparticle were quantified using flow cytometry.

Detection of Inflammation-Related Markers

Inflammatory and anti-inflammatory cytokine expressions were measured using quantitative real-time PCR (Bio-Rad, CFX 384), according to the manufacturer's protocol. FLS or J774 cells were seeded at a density of 5×10^5 per well in six-well plates. For the analysis of pro-inflammatory cytokines, the cells were pretreated with appropriate drugs for 2 h and then treated with 50 ng/mL of LPS or TNF-α for 12 h. For anti-inflammatory cytokines and M2 macrophage markers, cells were pretreated with 50 ng/mL of LPS or TNF-α for 2 h and then treated with appropriate compounds. Total RNA was extracted from FLS or J774 cells using QIAzol® lysis reagent (79,306, QIAGEN, Germany), followed by reverse transcription into cDNA using RT Premix (Promega, USA) at 45°C for 60 min and at 95°C for five min. The synthesized cDNA samples were analyzed for target genes using the primer sequences listed in Table S2, with *GAPDH* as the housekeeping gene. The cycle threshold (Ct) values were quantified using CFX 384 Real-Time PCR Detection System (Bio-Rad), and the $2^{-\Delta\Delta Ct}$ method was used to calculate the relative expression of each target gene.[44] For the detection of IL-22R, T cells were seeded at a density of 5×10^5 per well in 24-well plates. Cells were pretreated with 0.5 μg/mL of PLGA-MET-ICG for 2 h, followed by treatment with a 650 mW laser (LDH808, 808 nm wavelength) attached to a beam expander (Ronar-Smith), as shown in Figure S1, for 30s. After 2 h of incubation, total RNA was extracted as described previously.

Construction of CIA Models

All animal experiments were conducted in accordance with the guidelines of Gachon University's Center of Animal Care and Use (IRIS #:12919200). Four-to-six-week-old male DBA/1 mice weighing 20–25 g were purchased from Orient Bio (Korea). For acclimatization, mice were maintained in a climate-controlled, pathogen-free environment at 22 °C under 12 h light/ 12 h dark cycle for seven days. Arthritis was induced in mice according to the protocol described by Brand et al for the development of CIA mice models.[45] A mixture of complete Freund's adjuvant (100 μg of *Mycobacterium tuberculosis*; 7009, Chondrex, USA) and 100 μg of bovine type II collagen (20,021, Chondrex, USA) was subcutaneously introduced, followed by an injection of a mixture of incomplete Freund's adjuvant and 100 μg of bovine type II collagen after three weeks. After the initial signs of arthritis on day 28, mice were randomly assigned into the following five groups: saline, saline + laser, metformin, PLGA-MET, and PLGA-MET-ICG (n=5 per group).

Treatment of CIA Models and Evaluation of Arthritis Severity

The extent of RA was evaluated every five days based on a previously established guide for scoring arthritis severity.[45] Scores of 0, 1, 2, 3, and 4 indicate no visible inflammation, mild swelling of one or two toes, mild swelling of an entire paw or three or more inflamed toes, swelling of an entire paw, and severe swelling of an entire paw and all toes, respectively. At the start of treatment (day 28), each group had initial average arthritis scores between 2.8 and 3, and 10 mg/kg metformin was injected intraperitoneally twice per week for 21 days.[46,47] Each paw of the saline + laser and PLGA-MET-ICG groups were exposed to an 808 nm NIR laser (650 mW) for 60s on the day after the nanoparticle injection. At the end of the experiment, the mice were euthanized, and their tissues, organs, and blood samples were collected for further study. For histological analysis, two sets of inflamed joints from each group were fixed using 4% paraformaldehyde for three days at 4°C, followed by decalcification using a decalcifying solution (Sigma) for two weeks at room temperature. The decalcified ankle joints were paraffinized and then isolated to obtain slices with a thickness of 3 μm. The isolated tissues were stained with hematoxylin and eosin (H&E) and Safranin-O solution (Saf-O) to assess lymphocyte infiltration and cartilage damage, respectively. The kidney, spleen, heart, lung, and liver samples were collected and weighed to assess in vivo safety. Blood samples were collected from the eye sockets to evaluate the levels of alanine aminotransferase (ALT), aspartate aminotransferase (AST), creatinine, blood urea nitrogen (BUN), hemoglobin, red blood cells, platelets, and white blood cells.

Immunofluorescence Analysis

To analyze the features of RA, mice were euthanized 24 h after the first injection, and ankle joint samples were prepared as previously described. Sectioned samples were deparaffinized and incubated with the following primary antibodies:

CD3e (Invitrogen, USA; MA5-16762), IL-22R (Abcam, Cambridge, UK; ab203211), TNF-α (Abcam, Cambridge, UK; ab1793), F4/80 (Abcam, Cambridge, UK; ab6640), CD86 (Invitrogen, USA; 13–0862-82), and Dectin-1 (Abcam, Cambridge, UK; ab140039). Subsequently, the samples were treated with the following secondary antibodies: anti-mouse IgG Alexa Fluor 594 (Abcam, Cambridge, UK; ab150116) for TNF-α; anti-rabbit IgG Alexa Fluor 488 (Abcam, Cambridge, UK; ab150077) for CD86 and Dectin-1; anti-rat IgG Alexa Fluor 594 (Abcam, Cambridge, UK; ab150160) for F4/80; and anti-rat IgG Alexa Fluor 488 (Invitrogen, USA; PA1-84761) and anti-rabbit IgG Alexa Fluor 594 (Invitrogen, USA; A-11012) for IL-22R. The incubated samples were visualized under a confocal microscope (EVOS M7000; Invitrogen).

Immunological Assessment of Anti-RA Effects of PTT

T cells were isolated from the spleens of healthy DBA/1 mice and CIA models (control, saline, metformin, PLGA-MET, and PLGA-MET-ICG groups) after 24 days following the first injection using an isolation protocol described previously. Isolated T cells were labeled with anti-T-bet (Abcam, Cambridge, UK; ab953657) and anti-IL-17 (Abcam, Cambridge, UK; ab189377) antibodies targeting Th1 and Th-17, respectively. The proportion of Th-1 and Th-17 cells was measured by fluorescence-activated cell sorting.

Statistical Analysis

Statistical significance was analyzed using Student's *t*-test for two sample groups and one-way analysis of variance (ANOVA), followed by Tukey's multiple comparison test with $* p < 0.05$, $** p < 0.01$, *and* $*** p < 0.001$.

Results

Characterization of PLGA Nanoparticles

Metformin hydrochloride and ICG were conjugated to PLGA via emulsification and sonication (Figure 1a). Transmission electron microscopy (TEM) images revealed spherical structures with diameters of approximately 80 nm, confirming the successful formation of the PLGA-MET complexes (Figures 1b, S2). In UV-VIS, Metformin and ICG had characteristic absorbance peaks around 232 and 800 nm, respectively,[48,49] and the absorbance peaks near 232 and 800 nm for PLGA-MET and PLGA-MET-ICG (indicated by dashed lines) supported the presence of metformin and ICG in the resulting PLGA nanoparticles (Figure 1c). The successful loading of metformin and ICG in PLGA was further corroborated by Fourier Transform Infrared Spectroscopy (Figure S3). The average hydrodynamic sizes of the free PLGA, PLGA-MET, and PLGA-MET-ICG were 145, 176, and 180 nm, respectively (Figure 1d). The subsequent increase in hydrodynamic size was attributed to the loading of metformin and ICG into the free PLGA particles. The surface charge of free PLGA was negative due to the negatively charged carboxyl group, whereas free metformin and ICG exhibited relatively neutral surface charges (Figure 1d). Accordingly, the conjugation of neutral metformin to PLGA led to the development of PLGA-MET with an overall negative surface potential (Figure 1d). The light-absorbing properties of ICG were tested using thermal imaging. Notably, the treatment of PLGA-MET-ICG with NIR laser for five minutes increased the surrounding temperature by 6°C (Figure 1e and f). The release behavior of PLGA nanoparticles was characterized by an in vitro release study,[50] in which the NIR laser treatment led to a faster, greater release of nanoparticles in J774 cells (Figure 1g). Importantly, metformin was dissociated more readily in acidic environments that mimic those of inflamed joints.

Cellular Uptake of Nanoparticles

To understand how PLGA nanoparticles are engulfed by the target cells, the cellular uptake of PLGA by J774 cells was investigated (Figure 2a). Among many endocytic pathways, most polymeric nanoparticles pass the plasma membrane via three major pathways: caveolae-mediated endocytosis, clathrin-mediated endocytosis, and macropinocytosis.[51] Prior to treating J774 cells with endocytic pathway inhibitors, DiO, a green fluorescent dye, was encapsulated into PLGA as a visualizing agent. Subsequently, J774 cells were pretreated with inhibitors of caveolae-mediated endocytosis (GEN), clathrin-mediated endocytosis (CPZ), and macropinocytosis (EIPA) to identify the major endocytic pathways of the

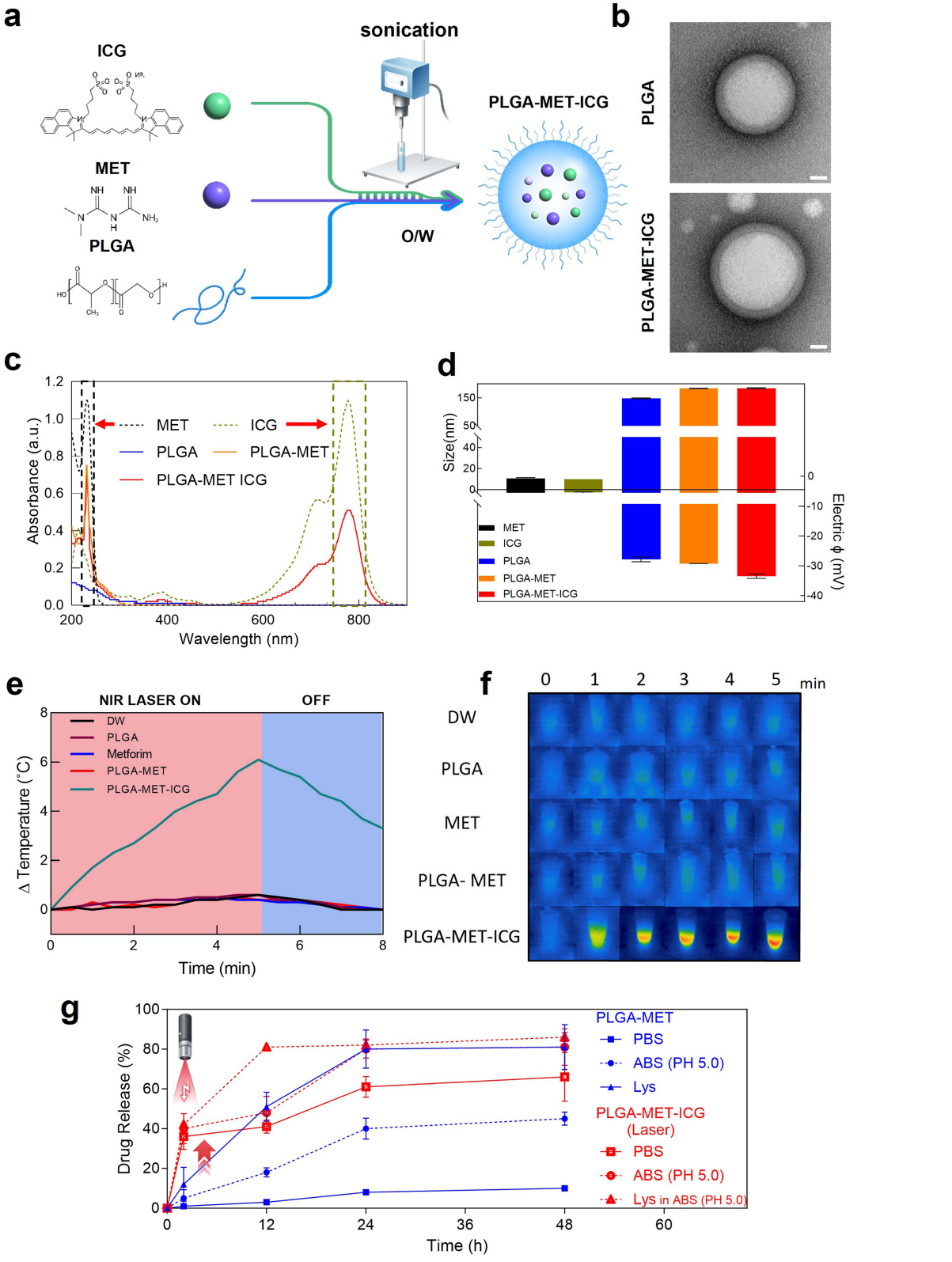

Figure 1 Characterization of physiochemical properties of synthesized nanodrugs. (**a**) Synthesis of PLGA-MET and PLGA-MET-ICG. Metformin and ICG were dissolved in distilled water and simultaneously conjugated to PLGA via emulsification. (**b**) TEM images of PLGA with and without metformin and ICG encapsulation. The visible change in morphology suggests the successful encapsulation of metformin and ICG. Scale bar = 20 nm. (**c**) UV-VIS analysis showing characteristic peaks for metformin (232 nm) and ICG (790 nm). (**d**) Average hydrodynamic sizes and zeta (electric) potentials of the synthesized nanodrugs. An increase of 31 nm and 4 nm in the average size was observed after the conjugation of metformin and ICG, respectively. (**e**) Changes in the temperature of solutions with and without ICG upon treatment with NIR. (**f**) Thermal imaging of NIR laser absorption in conjunction with 0.5 μg/mL of PLGA-MET-ICG. An increase in temperature is indicated by bright red areas. (**g**) In vitro release study of PLGA-MET and PLGA-MET-ICG performed in three different conditions, PBS, ABS (PH 5.0), and Lysozyme in ABS (PH 5.0).

https://doi.org/10.2147/IJN.S438388 DovePress

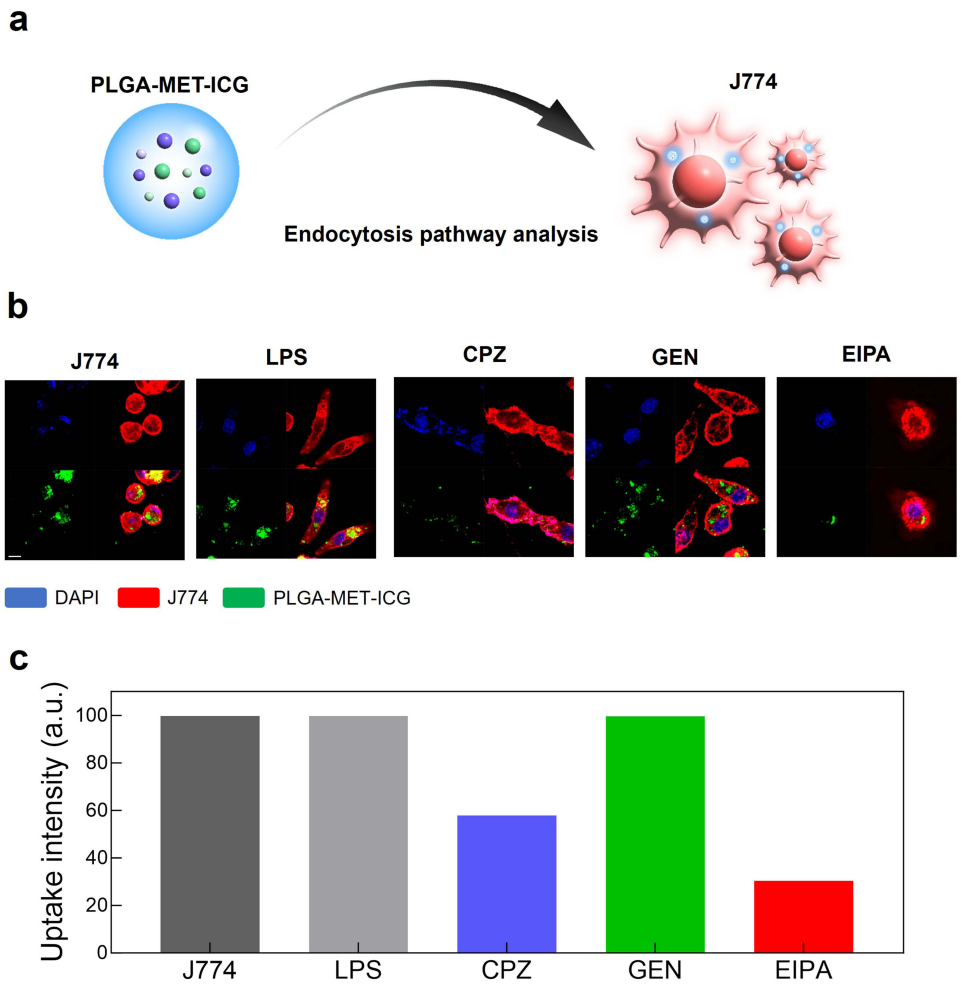

Figure 2 Analysis of the uptake of PLGA-DiO in J774 cells. (**a**) Schematic representation of the investigation of endocytic pathway associated with PLGA-MET-ICG in J774 cells. (b) Live cell imaging illustrating the uptake of PLGA-DiO in J774 cells stimulated by 50 ng/mL of LPS. Macrophage cells were incubated with three different types of uptake inhibitors, EIPA (macropinocytosis), GEN (caveolae-mediated endocytosis), and CPZ (clathrin-mediated endocytosis). The treatment with EIPA and CPZ influenced the uptake of PLGA-DiO, whereas GEN had no effect on the intracellular localization of the nanoparticle. (**c**) Quantification of FACS results. Scale bar = 20 μm.

nanodrug. Live cell imaging revealed that the nanodrug primarily penetrated the cell via macropinocytosis and clathrin-mediated endocytosis, as indicated by the relative lack of co-localization of the fluorescent signals (Figure 2b). Fluorescence-activated cell sorting (FACS) further corroborated that the nanoparticles entered the cells via clathrin-mediated endocytosis and macropinocytosis but depended more heavily on macropinocytosis (Figure 2c).

Anti-Inflammatory Effects of PLGA-MET in vitro

Given the known anti-inflammatory properties of metformin, its ability to downregulate inflammation when encapsulated into PLGA nanoparticles has been evaluated.[18] To test this hypothesis, inflammatory models in which J774 cells and FLS were stimulated by LPS or TNF-α to develop M1 phenotype, were treated with free PLGA, metformin, and PLGA-MET. Upon treatment, the mRNA expression levels of pro-inflammatory cytokines (IL-1β, IL-6, and TNF-α) were reduced by both free metformin and PLGA-MET in a concentration-dependent manner in J774 (Figure 3b). The most profound effect was observed in TNF-α levels, in which the cytokine expression was significantly reduced. Likewise, metformin and PLGA-MET increased the expression of anti-inflammatory cytokines IL-10 and IL-4 (Figure 3c). However, the two compounds did not increase the level of IL-10 in a concentration-dependent manner. Moreover, the treatments induced the repolarization of M1 to M2 macrophages, as shown by the increase in the level of the M2 macrophage marker, Arg-1 (Figure 3c).[52] Upon 2 μg/mL treatment of PLGA-MET, the expression of Arg-1 almost increased by 10 folds in J774

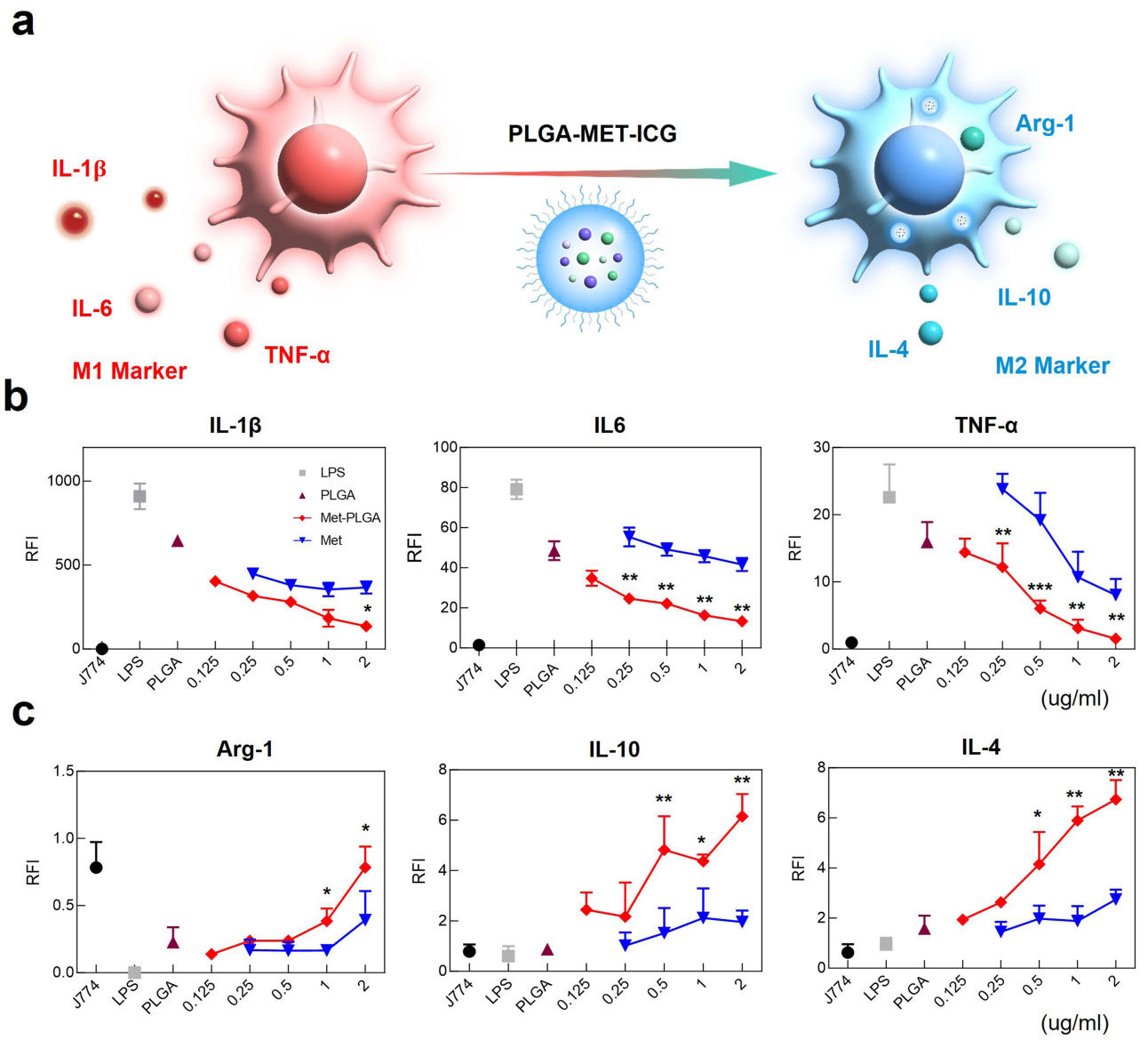

Figure 3 Evaluation of anti-inflammatory effects of PLGA-MET on J774 via real-time PCR. (**a**) Illustration of the effect of the nanodrug on inflammatory cytokines and macrophage polarization. (**b**) The effect of PLGA-MET on pro-inflammatory cytokines (IL-1β, IL-6, and TNF- α). J774 cells were stimulated with 50 ng/mL of LPS and then incubated with different compounds. PLGA-MET led to the downregulation of the expression of all inflammatory cytokines. (**c**) The effect of PLGA-MET on anti-inflammatory markers (Arg-1, IL-10, and IL-4). J774 cells were first incubated with appropriate chemicals and then stimulated with 50 ng/mL of LPS. Treatment with PLGA-MET led to a higher increase in the expression of anti-inflammatory cytokines than that observed with free metformin. The data is presented as mean ± SEM (n = 3). *p < 0.05, **p < 0.01, and ***p < 0.001.

cells. Similar trends were observed in FLS, in which the treatment of PLGA-MET notably decreased the expression of pro-inflammatory cytokines (Figure 4). In all aspects, PLGA-MET exhibited more potent anti-RA effects than free metformin, even at much lower concentrations. This observation highlights the importance of encapsulating metformin into PLGA particles to allow metformin to effectively penetrate the plasma membrane.

Inactivation of IL-22 Receptor by PLGA-MET Combined with PTT

The inhibitory effects of PLGA-MET-ICG on IL-22R were investigated using T cells present in the mouse spleen. Isolated T cells were incubated at 37°C for 2 h with 0.5 μg/mL and then treated with NIR laser (808 nm) for up to five minutes. Compared to T cells that were not incubated with PLGA-MET-ICG, the expression of IL-22R was significantly reduced in T cells pretreated with the nanodrug after NIR irradiation (Figure 5b). Furthermore, PLGA-MET-ICG-based

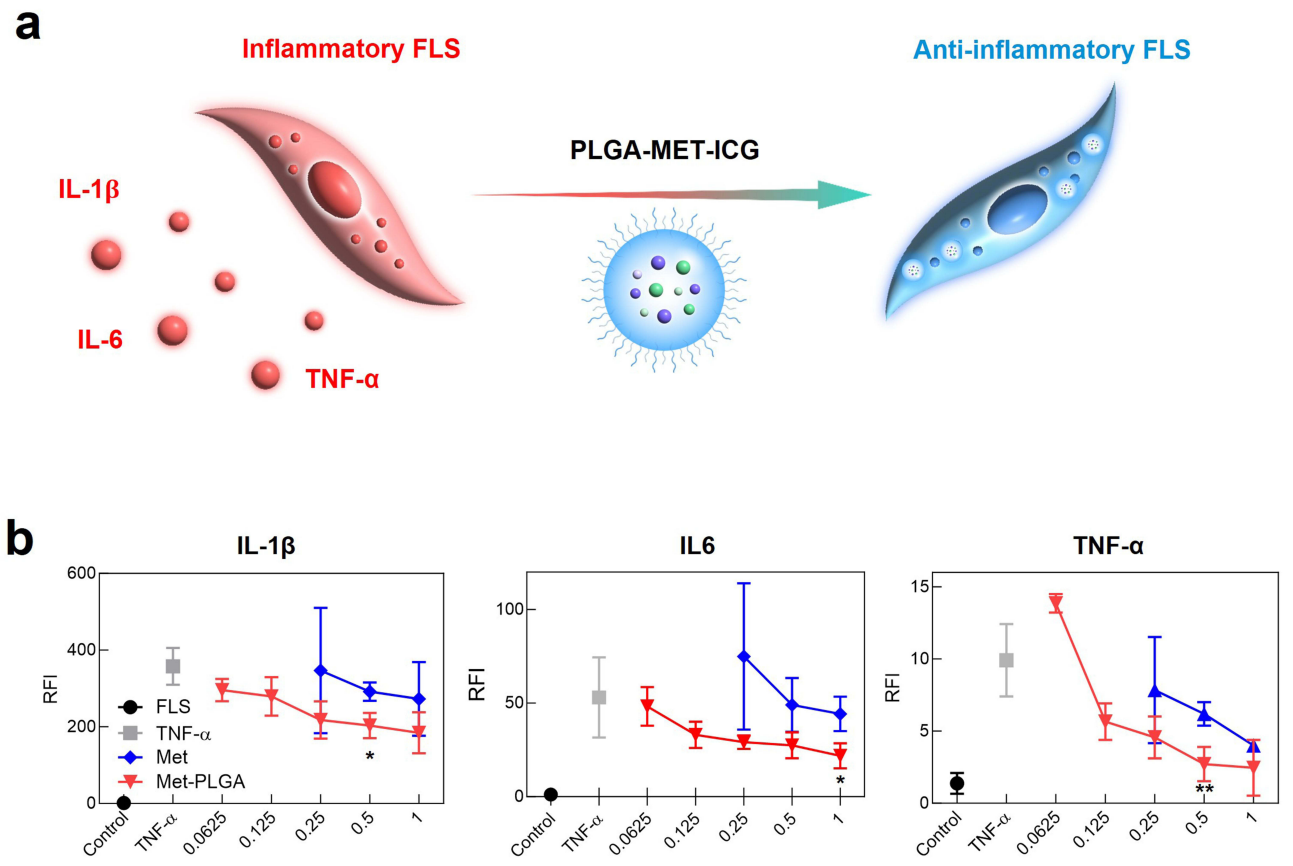

Figure 4 Evaluation of anti-inflammatory effects PLGA-MET on FLS via real-time PCR. (**a**) Illustration of the effects of the nanodrug on inflammatory cytokines and macrophage polarization. (**b**) The effect of PLGA-MET on pro-inflammatory cytokines (IL-1β, IL-6, and TNF- α). FLS were stimulated with 50 ng/mL TNF-α and then incubated with different compounds. PLGA-MET led to the downregulation of the expression of all inflammatory cytokines. The data are presented as mean ± SEM (n = 3). *$p < 0.05$ and **$p < 0.01$.

PTT downregulated the expression of IL-22R in a time-dependent manner, with the relative expression of IL-22R reaching almost zero after five minutes (Figure 5b). On the other hand, no notable changes in the level of IL-22R were seen in the untreated T cells, illustrating the importance of ICG's role as a photothermal agent. To verify whether PTT specifically targeted IL-22R, we measured the changes in the expression of CD23, a housekeeping receptor gene in mammals. No changes in the level of CD23 upon NIR irradiation would suggest IL-22R's unique thermal responsiveness. After laser treatment, the relative levels of CD23 in T cells remained primarily unchanged, indicating that PTT only targets IL-22R (Figure 5b). These results demonstrate that IL-22R, an important precursor of Th-17 cells, can be specifically downregulated via PTT, ultimately suggesting that the PLGA-MET-ICG treatment with PTT can greatly counteract inflammation in joints.

Anti-RA Efficacy of PLGA-MET with PTT

Arthritic severity scores in the CIA mouse model were measured to evaluate the anti-RA effects of the nanodrug in vivo. After initial signs of arthritis in CIA models, the mice were administered intraperitoneal injections of PBS, free metformin, PLGA-MET, and PLGA-MET-ICG (10 mg metformin/kg) twice per week (Figure 6a).[53] Seven days after the first injection, clear reductions in the arthritic scores of the PLGA-MET- and PLGA-MET-ICG-treated mice were observed (Figure 6c). Minimal reductions in inflammation were observed in the metformin- and saline-treated groups, whereas the arthritic scores increased in the saline + laser-treated group. The trend observed in the saline + laser group demonstrates that PTT requires a photothermal agent to be delivered to the sites of inflammation. The paw scores for the PLGA-MET- and PLGA-MET-ICG-treated groups decreased at a similar rate, but the PLGA-MET-ICG-treated group had the lowest average arthritic score at the end of the experiment (Figure 6c). These findings indicate that PTT enhances

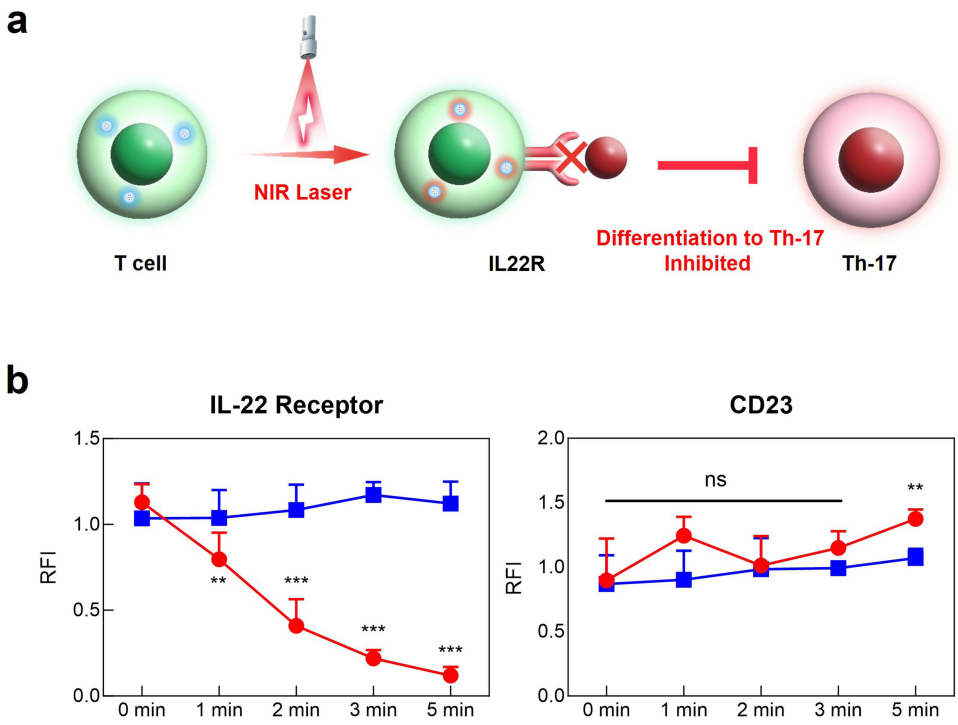

Figure 5 Thermal inactivation of IL-22R in mouse T cells. (**a**) Schematic representation of amelioration of RA via thermal inactivation. (**b**) Analysis of mRNA expression of IL-22R and CD23 via real-time PCR. Mouse T cells were isolated from the spleens of healthy DBA/1 mice and then treated with PLGA-MET-ICG, followed by NIR laser (808 nm) treatment. The expression of IL-22R and the duration of PTT displayed a strong, negative correlation. CD23, a receptor housekeeping gene, was used to confirm the specific thermal inactivation of IL-22R. The data are presented as mean ± SEM (n = 3). $^{**}p < 0.01$ and $^{***}p < 0.001$.

the anti-inflammatory effects of PLGA-MET. The anti-inflammatory effects of PLGA-MET with PTT were also visible in the paw images, in which the paws and toes of the PLGA-MET- and PLGA-MET-ICG-treated groups showed reduced swelling over time (Figure S4). Spleen samples were collected at the end of the experiment to further evaluate the efficacy of the nanodrugs. Spleen samples were used to examine the numbers of Th1 and Th-17, which have been studied as markers of RA. FACS results revealed that the percentages of Th1 and Th-17 in the spleen were significantly decreased in the PLGA-MET-ICG-treated group (Figure 7). The levels of Th-1 and Th-17 were also reduced in the PLGA-MET-treated group; however, the levels were higher than those in the PLGA-MET-ICG group. Furthermore, the percentages of Th1 and Th-17 in the metformin-treated group remained unchanged or increased compared to those in healthy mice.

Immunohistological Evaluation of Anti-Inflammatory Effects

Immunohistochemical analyses were conducted to further confirm the anti-RA effects of the nanodrugs (Figure 6b). The mice were euthanized 24 days after the first injection, and the inflamed joint slices were prepared and stained with hematoxylin and eosin (H&E), safranin-O (Saf-O), M1 and M2 macrophage markers, TNF-α, and IL-22R. H&E staining revealed hyperplastic synovium in the ankle joints of mice that were not treated with NIR. In contrast, H&E staining of the PLGA-MET-ICG-treated group revealed a non-hyperplastic synovium that almost resembled that of healthy mice. Furthermore, Saf-O staining illustrated notable cartilage destruction (as indicated by narrowing of the joint space) in the non-NIR-treated groups, whereas cartilage samples of the PLGA-MET-ICG-treated groups showed no sign of joint space narrowing. Immunofluorescence images revealed clear reductions in TNF-α levels in joint samples treated with PLGA-MET-ICG and PTT compared to those in other groups (Figure 8a). Similarly, confocal microscopy images showed that PLGA-encapsulated metformin promoted M1 → M2 macrophage repolarization (Figure 8b). Clear reductions in CD86 (M1 marker) and elevations in Dectin-1 (M2 marker) levels were visible in joint samples treated with PLGA-MET and PLGA-MET-ICG. Furthermore, immunofluorescence images showed a decrease in IL-22R only in joint samples treated with PLGA-MET-ICG and PTT (Figure 8c).

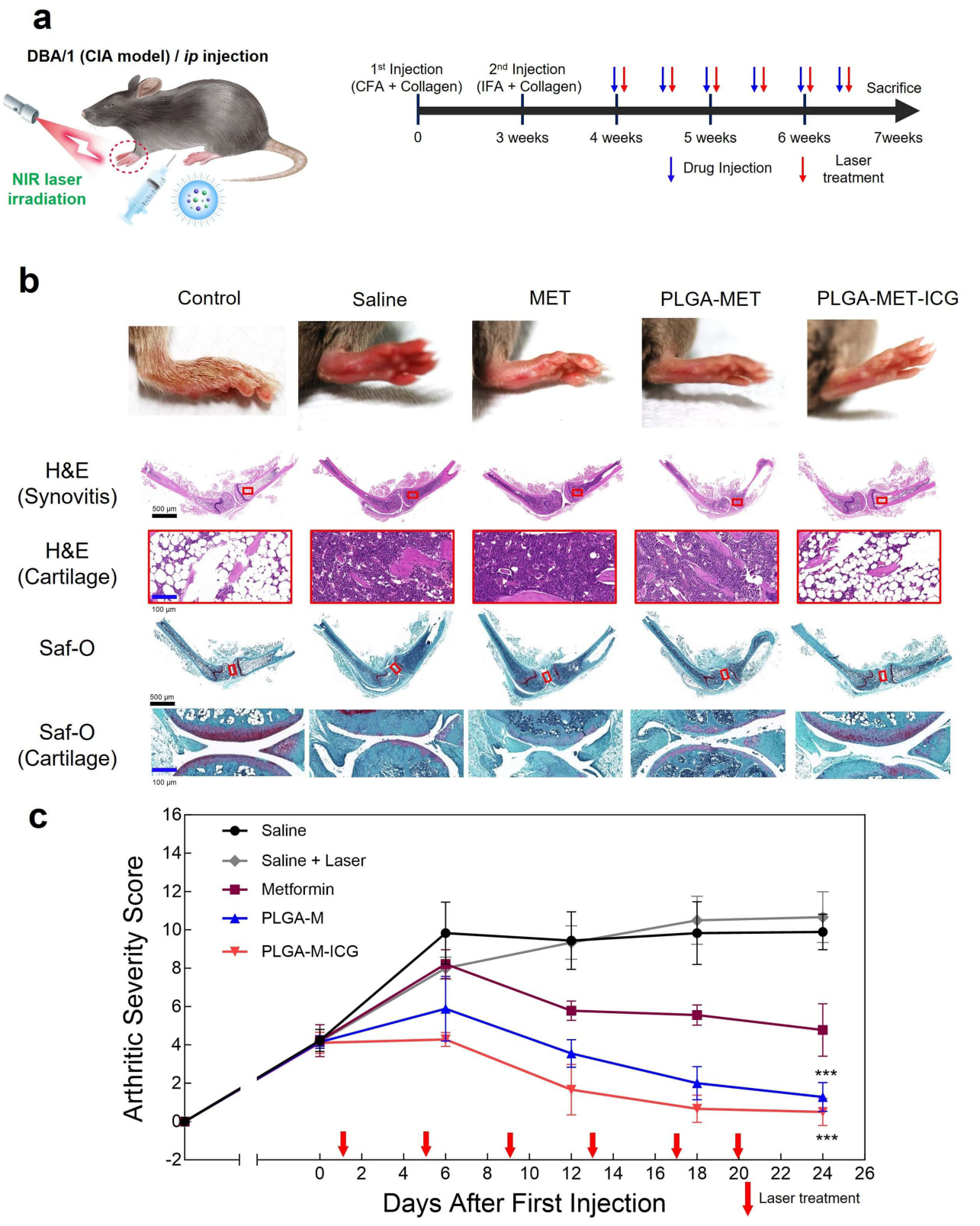

Figure 6 Anti-RA effects of PLGA-MET-ICG with PTT on CIA mice models. (**a**) Schematic illustration of the animal experiment. (**b**) Representative images of paws, hematoxylin & eosin (H&E) staining, and Safranin-O (Saf-O) staining. Joint samples were obtained from healthy mice and CIA mice treated with saline, free metformin, PLGA-MET (10 mg/kg), and PLGA-MET-ICG (10 mg/kg). (**c**) Arthritic severity scores of the saline- saline + laser-, metformin-, PLGA-MET-, and PLGA-MET-ICG-treated groups. The injection of PLGA-MET and PLGA-MET-ICG (with PTT) significantly reduced arthritic severity scores; the PLGA-MET-ICG group exhibited the lowest score at the end of the experiment. CIA scores were recorded five times over 24 days after the first injection. The data are presented as mean ± SEM (n = 4). ***$p < 0.001$.

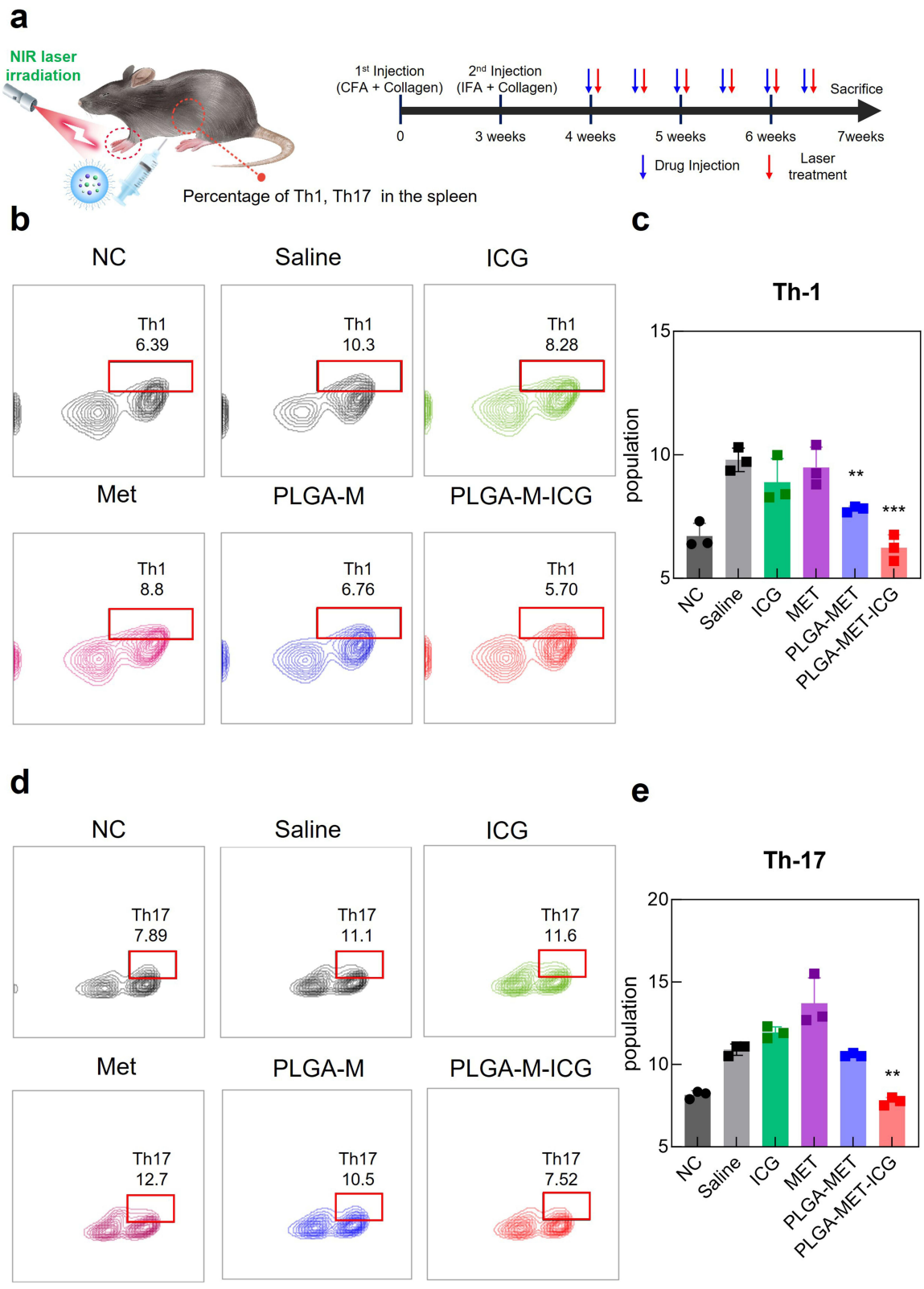

Figure 7 Analysis of Th-1 and Th-17 expression in CIA mice models via flow cytometry. (**a**) Illustration of the experimental setup. T cells were isolated from spleens of CIA mice models at the end of the drug treatment. Anti-T-bet and anti-IL-17 were used as markers for Th-1 and Th-17, respectively. (**b** and **c**) The relative population of Th-1 cells in CIA mice models. (**d** and **e**) The relative population of Th-17 cells in CIA mice models. The levels of Th-1 and Th-17 were significantly reduced in the PLGA-MET-ICG group. The data are presented as mean ± SEM (n = 4). $^{**}p < 0.01$, and $^{***}p < 0.001$.

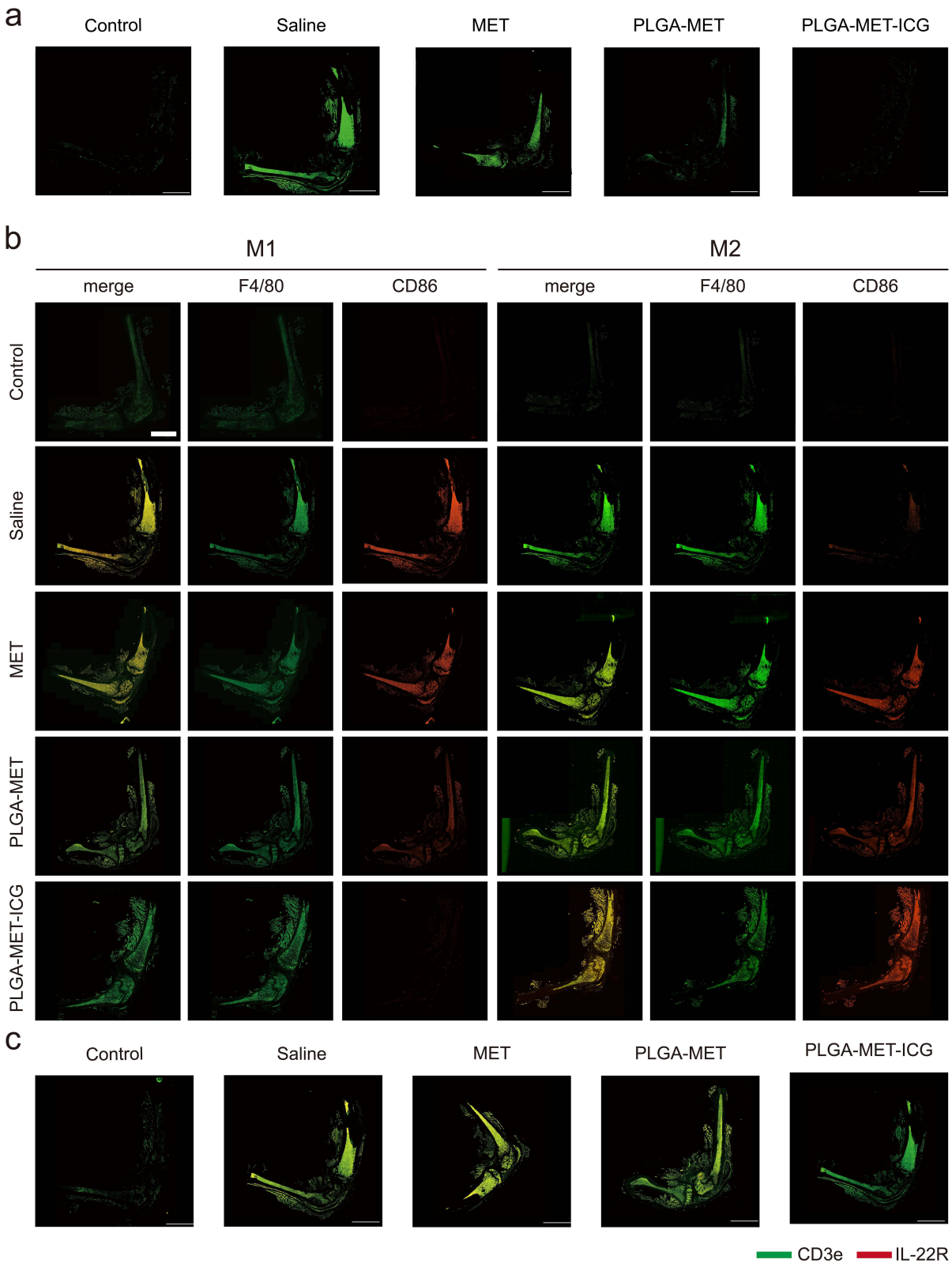

Figure 8 Immunofluorescence analysis. Joint samples were isolated and incubated with appropriate antibodies to visualize the progression of RA in inflamed regions via confocal microscopy. (**a**) Immunofluorescence staining for TNF-α. (**b**) Evaluation of M1 → M2 macrophage repolarization. F4/80 was used as a macrophage marker, CD86 as an M1 marker, and Dectin-1 as an M2 marker. (**c**) Staining images for IL-22R. A clear decrease in fluorescence was observed in the PLGA-MET-ICG group. (Scale bar, 2000 μm).

In vivo Safety Evaluation

Major organs (liver, kidney, heart, spleen, and lungs) and blood samples were analyzed to assess the safety of PLGA nanoparticles (Figures S5 and S6). The injection of PLGA particles did not lead to significant changes in the mass of the major organs. Moreover, the levels of alanine aminotransferase (ALT), aspartate aminotransferase (AST), blood urea nitrogen (BUN), creatine, hemoglobin, red blood cells, and platelets remained consistent across the different treatment types.

Discussion

Despite recent progress in comprehending the pathogenesis of RA, it continues to pose a significant threat to the overall health of numerous individuals. Many attempts have been made to attenuate autoimmune arthritis; however, these are complicated by poor pharmacokinetic properties and side effects of therapeutics, highlighting the need for novel anti-RA agents.[54,55] Recently, drug repositioning has emerged as a gateway to transform and optimize pre-existing therapeutics for new uses. This study aimed to exploit drug repositioning to develop an effective and novel agent for the attenuation of RA. The search led to the examination of metformin, an antidiabetic agent that has been reported to reduce inflammation.[22,23] Despite its anti-inflammatory properties, metformin has not been used to treat RA because it readily dissociates in the human body owing to its strong hydrophilic properties. To overcome this issue, metformin was encapsulated in poly PLGA nanoparticles to synthesize PLGA-MET with a mean diameter significantly smaller than those reported in previous studies, which may serve as an advantage when the nanodrug enters the target cells (Figure 1d).[56] The encapsulation of metformin into nanoparticles successfully protected it from degradation and allowed the nanodrug to cross the membrane via macropinocytosis and clathrin-mediated endocytosis (Figure 2). Therefore, the findings suggest that the encapsulation of metformin into PLGA can help overcome the poor cellular delivery of metformin owing to its hydrophilic amine and imine groups.[27,28]

Cytokines are critical signaling molecules that can either exacerbate or downregulate inflammation.[57] Pro-inflammatory cytokines are produced by M1 macrophages and FLS, and are involved in the up-regulation of inflammatory responses that cause pain and swelling in inflamed regions.[58] The major pro-inflammatory cytokines involved in RA include IL-1β, IL-6, and TNF-α.[3] In contrast, anti-inflammatory cytokines, such as IL-10 and IL-4 exhibit potent anti-inflammatory effects by acting as inhibitors of pro-inflammatory cytokines or downregulating the transcription of pro-inflammatory molecules.[59] Therefore, suppressing the expression of pro-inflammatory cytokines while increasing the expression of anti-inflammatory cytokines is crucial for the treatment of RA, as demonstrated by Khang et al.[51] In this study, PLGA-MET exhibited potent anti-inflammatory effects at the cellular level by downregulating the expression of major pro-inflammatory cytokines, upregulating the expression of anti-inflammatory cytokines, and inducing the polarization of M1 to M2 macrophages (Figures 3 and 4). Importantly, PLGA-MET consistently exhibited more potent anti-RA effects than free metformin, which highlights the importance of the use of PLGA nanoparticles as a drug delivery system. The findings indicate that PLGA-MET can mitigate the current side effects of metformin in patients with RA, which stem from the administration of high, repeated doses of metformin to achieve anti-RA outcomes.[16,17] Interestingly, free PLGA also showed low to moderate anti-inflammatory effects (especially on the three pro-inflammatory cytokines, calling for the need for further investigation into the intrinsic behavior of PLGA in the inflammatory sites (Figure 3a and b).

Apart from inflammatory cytokines, Th-17 is also a key player in the perpetuation of RA.[11] Th-17 produces and activates IL-17, a potent pro-inflammatory cytokine that recruits neutrophils.[11] Hence, inhibiting the production of Th-17 can remarkably ameliorate symptoms of RA. However, previous studies have reported difficulties in downregulating Th-17 in animal models, which has led to the examination of the suppression of the expression of Th-17 precursors.[9,23,60] To first confirm the increase in the Th-17 population in the inflamed synovium, joint samples of collagen-induced arthritis (CIA) mice models were analyzed (Figure S7). As expected, a sharp increase in the levels of Th-17 was observed, corroborating that the inhibition of Th-17 can ameliorate RA. While testing various approaches to inactivate Th-17 precursors, the thermal responsiveness of the IL-22 receptor (IL-22R), an important downstream regulator of Th-17, has been discovered.[41] Specifically, creating a hyperthermal environment via a NIR laser downregulates the expression of IL-22R. To induce the development of hyperthermal environments in the inflamed regions, ICG was added to PLGA-MET,

in which the dye displayed promising thermal abilities (Figure 1e and f). As expected, PLGA-MET-ICG-incubated T cells displayed a decrease in IL-22R expression after laser treatment (Figure 5b). Furthermore, no changes in the expression of CD 23 indicated that NIR laser treatment specifically inactivates IL-22R (Figure 5b). This is a crucial finding because it enables the downregulation of inflammation in a spatiotemporal manner via PTT. However, no experiments were performed to decipher the molecular mechanism underlying the role of IL-22R in the perpetuation of RA, necessitating further investigation.

Based on such findings, the anti-RA efficacy of PLGA-MET with PTT was tested in animal models. The LDH808 Laser (650 mW, power 975 mJ / cm^2) was chosen as the source of NIR to maintain a balance between reaching the target area and avoiding damage in healthy cells.[61] The combination of PTT and PLGA-MET treatment led to a significant reduction in inflammation and cartilage damage in the joints of CIA mice, to the point where the paw samples of PLGA-MET-ICG-treated mice and healthy mice were almost indistinguishable (Figure 6 and S4). Notably, although the free metformin-treated group also showed moderate anti-inflammatory effects, the extent of the reduction in swelling was much lower than that in the two PLGA-MET-treated groups. The limited efficacy of free metformin was clearly visible in the paw images in which three or more toes remained swollen at the end of the experiment (Figure 6b, S4). This observation highlights the inadequacy of metformin alone in mitigating inflammation, underscoring the significance of employing PLGA as a drug carrier to enhance plasma membrane penetration.[31] The analysis of Th-1 and Th-17 levels in CIA mice spleens revealed the levels of these cells in the PLGA-MET-ICG group were almost as low as those in healthy mice (Figure 7). Similar to Th-17 cells, Th-1 cells recruit pro-inflammatory cytokines (IFN-γ and IL-2) and stimulate bone destruction by producing osteoclasts.[62,63] These results demonstrate that the incorporation of PTT into PLGA-MET was crucial for achieving the most potent anti-RA effects. The in vivo safety analyses indicated the absence of cytotoxic effects of the nanodrugs in mouse models (Figures S5 and S6). This indicates the intraperitoneal injection of nanoparticles did not affect healthy tissues or organs. However, some abnormalities were observed in the white blood cells, specifically in the monocytes, basophils, and eosinophils (Figure S6). These results may be attributed to the inherent differences among individual CIA mouse models. However, follow-up experiments are required to explain these phenomena, especially because these white blood cell indicators are linked to the development of inflammatory diseases.[64]

The nanodrug and PTT's anti-inflammatory effects were also observed in immunohistological analyses. In the joint samples of CIA mice, PLGA-MET-ICG-treated groups showed no sign of joint space narrowing (Figure 6b). Joint space narrowing serves as an indicator of advanced arthritis because cartilage inflammation leads to a reduction in the gap between the bones within a joint.[65] Immunofluorescence analysis revealed three major trends in the joints of PLGA-MET - and PLGA-MET-ICG-treated mice: 1) the reduction of TNF-α, a key pro-inflammatory cytokine that perpetuates RA, 2) the increase in Dectin-1 and decrease in CD86 levels, and 3) the decrease in IL-22R signals (Figure 8). The observation that anti-RA effects were solely apparent in the two PLGA samples underscores the significance of encapsulating metformin within the nanoparticle structure. Also, the level of IL-22R decreased the most in the PLGA-MET-ICG-treated joints, demonstrating that the incorporation of PTT into PLGA-MET was crucial for achieving the most potent anti-RA effects.

Conclusion

In summary, we developed PLGA-MET-ICG as a powerful anti-RA drug, in which its anti-inflammatory effects can be maximized by PTT. This study presents two major conclusions: 1) the use of PLGA nanoparticles as a drug carrier is important in delivering metformin to target cells and 2) the incorporation of PTT is imperative to realize optimum anti-RA effects. Although this study did not outline the molecular mechanism of IL-22R thermal inactivation, it can be reasonably hypothesized that PTT downregulates the expression of IL-22R, causing a reduction in the Th-17 population. Further studies are required to elucidate the role of IL-22R in RA pathogenesis. Nevertheless, this study establishes a crucial, foundational step in harnessing the thermal attributes of immune cell regulators and nanotechnology to forge innovative and potent therapeutic avenues for addressing RA.

Acknowledgments

This work was supported by the Basic Science Research Program of the National Research Foundation of Korea (NRF-2022M3A9H1014123 and NRF 2021R1F1A1056332).

Disclosure

The authors declare that they have no competing financial interests or personal relationships that may have influenced the work reported in this study.

References

1. Smith E, Hoy DG, Cross M, et al. The global burden of other musculoskeletal disorders: estimates from the Global Burden of Disease 2010 study. *Ann Rheumatic Dis*. 2014;73(8):1462. doi:10.1136/annrheumdis-2013-204680
2. Aletaha D, Smolen JS. Diagnosis and Management of Rheumatoid Arthritis: a Review. *JAMA*. 2018;320(13):1360–1372. doi:10.1001/jama.2018.13103
3. Scott DL, Wolfe F, Huizinga TWJ. Rheumatoid arthritis. *Lancet*. 2010;376(9746):1094–1108. doi:10.1016/S0140-6736(10)60826-4
4. Feldmann M, Brennan FM, Maini RN. Role of cytokines in rheumatoid arthritis. *Ann Rev Immunol*. 1996;14(1):397–440.
5. Cutolo M, Campitiello R, Gotelli E, Soldano S. The Role of M1/M2 Macrophage Polarization in Rheumatoid Arthritis Synovitis. *Front Immunol*. 2022;13:867260. doi:10.3389/fimmu.2022.867260
6. Pham CTN. Nanotherapeutic approaches for the treatment of rheumatoid arthritis. *WIREs Nanomed Nanobiotechnol*. 2011;3(6):607–619. doi:10.1002/wnan.157
7. Choy EH, Panayi GS. Cytokine pathways and joint inflammation in rheumatoid arthritis. *N Engl J Med*. 2001;344(12):907–916. doi:10.1056/NEJM200103223441207
8. Bettelli E, Oukka M, Kuchroo VK. T(H)-17 cells in the circle of immunity and autoimmunity. *Nat Immunol*. 2007;8(4):345–350. doi:10.1038/ni0407-345
9. Yasuda K, Takeuchi Y, Hirota K. The pathogenicity of Th17 cells in autoimmune diseases. *Semin Immunopathol*. 2019;41(3):283–297. doi:10.1007/s00281-019-00733-8
10. Bartok B, Firestein GS. Fibroblast-like synoviocytes: key effector cells in rheumatoid arthritis. *Immunol Rev*. 2010;233(1):233–255. doi:10.1111/j.0105-2896.2009.00859.x
11. Tesmer LA, Lundy SK, Sarkar S, Fox DA. Th17 cells in human disease. *Immunol Rev*. 2008;223(1):87–113. doi:10.1111/j.1600-065X.2008.00628.x
12. Bush KA, Farmer KM, Walker JS, Kirkham BW. Reduction of joint inflammation and bone erosion in rat adjuvant arthritis by treatment with interleukin-17 receptor IgG1 Fc fusion protein. *Arthritis Rheumatism*. 2002;46(3):802–805. doi:10.1002/art.10173
13. Nakae S, Nambu A, Sudo K, Iwakura Y. Suppression of immune induction of collagen-induced arthritis in IL-17-deficient mice. *J Immunol*. 2003;171(11):6173–6177.
14. Lubberts E, Koenders MI, Oppers-Walgreen B, et al. Treatment with a neutralizing anti-murine interleukin-17 antibody after the onset of collagen-induced arthritis reduces joint inflammation, cartilage destruction, and bone erosion. *Arthritis Rheumatism*. 2004;50(2):650–659.
15. Fang H, Sha Y, Yang L, et al. Macrophage-Targeted Hydroxychloroquine Nanotherapeutics for Rheumatoid Arthritis Therapy. *ACS Appl Mater Interfaces*. 2022;14(7):8824–8837. doi:10.1021/acsami.1c23429
16. Wang W, Zhou H, Liu L. Side effects of methotrexate therapy for rheumatoid arthritis: a systematic review. *Eur. J. Med. Chem.* 2018;158:502–516. doi:10.1016/j.ejmech.2018.09.027
17. McConkey B, Amos R, Durham S, Forster P, Hubball S, Walsh L. Sulphasalazine in rheumatoid arthritis. *Br Med J*. 1980;280(6212):442–444.
18. Gharib M, Elbaz W, Darweesh E, Sabri NA, Shawki MA. Efficacy and Safety of Metformin Use in Rheumatoid Arthritis: a Randomized Controlled Study. *Front Pharmacol*. 2021;12:726490. doi:10.3389/fphar.2021.726490
19. Pareek S, Huang Y, Nath A, Huang RS. Chapter 6 - The success story of drug repurposing in breast cancer. In: To KKW, Cho WCS, editors. *Drug Repurposing in Cancer Therapy*. Academic Press; 2020:173–190.
20. Bailey CJ, Turner RC. Metformin. *N Engl J Med*. 1996;334(9):574–579.
21. Ursini F, Russo E, Pellino G, et al. Metformin and Autoimmunity: a "New Deal" of an Old Drug. *Front Immunol*. 2018:9. doi:10.3389/fimmu.2018.01236
22. Son H-J, Lee J, Lee S-Y, et al. Metformin attenuates experimental autoimmune arthritis through reciprocal regulation of Th17/Treg balance and osteoclastogenesis. *Mediators Inflammation*. 2014;2014:656.
23. Kang KY, Kim Y-K, Yi H, et al. Metformin downregulates Th17 cells differentiation and attenuates murine autoimmune arthritis. *Int Immunopharmacol*. 2013;16(1):85–92.
24. O'Neill LA, Hardie DG. Metabolism of inflammation limited by AMPK and pseudo-starvation. *Nature*. 2013;493(7432):567.
25. Chen K, Lin ZW, He SM, et al. Metformin inhibits the proliferation of rheumatoid arthritis fibroblast-like synoviocytes through IGF-IR/PI3K/AKT/m-TOR pathway. *Biomed Pharmacother*. 2019;115:108875. doi:10.1016/j.biopha.2019.108875
26. Bouriche S, Alonso-García A, Cárceles-Rodríguez CM, Rezgui F, Fernández-Varón E. An in vivo pharmacokinetic study of metformin microparticles as an oral sustained release formulation in rabbits. *BMC Vet Res*. 2021;17(1):315. doi:10.1186/s12917-021-03016-3
27. Graham GG, Punt J, Arora M, et al. Clinical pharmacokinetics of metformin. *Clin Pharmacokinet*. 2011;50(2):81–98. doi:10.2165/11534750-000000000-00000
28. Smith DA, Beaumont K, Maurer TS, Di L. Relevance of Half-Life in Drug Design. *J Med Chem*. 2018;61(10):4273–4282. doi:10.1021/acs.jmedchem.7b00969
29. Chinnaiyan SK, Deivasigamani K, Gadela VR. Combined synergetic potential of metformin loaded pectin-chitosan biohybrids nanoparticle for NIDDM. *Int J Biol Macromol*. 2019;125:278–289.

30. Prasad LK, O'Mary H, Cui Z. Nanomedicine delivers promising treatments for rheumatoid arthritis. *Nanomedicine*. 2015;10(13):2063–2074. doi:10.2217/nnm.15.45
31. Couvreur P. Nanoparticles in drug delivery: past, present and future. *Adv. Drug Delivery Rev.* 2013;65(1):21–23. doi:10.1016/j.addr.2012.04.010
32. Sánchez A, Mejía SP, Orozco J. Recent Advances in Polymeric Nanoparticle-Encapsulated Drugs against Intracellular Infections. *Molecules*. 2020;25(16). doi:10.3390/molecules25163760
33. Huang R, Zhang C, Bu Y, et al. A multifunctional nano-therapeutic platform based on octahedral yolk-shell Au NR@CuS: photothermal/photodynamic and targeted drug delivery tri-combined therapy for rheumatoid arthritis. *Biomaterials*. 2021;277:121088. doi:10.1016/j.biomaterials.2021.121088
34. Shirata C, Kaneko J, Inagaki Y, et al. Near-infrared photothermal/photodynamic therapy with indocyanine green induces apoptosis of hepatocellular carcinoma cells through oxidative stress. *Sci Rep*. 2017;7(1):13958. doi:10.1038/s41598-017-14401-0
35. Wilczewska AZ, Niemirowicz K, Markiewicz KH, Car H. Nanoparticles as drug delivery systems. *Pharmacol Rep*. 2012;64(5):1020–1037. doi:10.1016/S1734-1140(12)70901-5
36. Vyawahare A, Prakash R, Jori C, Ali A, Raza SS, Khan R. Caffeic Acid Modified Nanomicelles Inhibit Articular Cartilage Deterioration and Reduce Disease Severity in Experimental Inflammatory Arthritis. *ACS Nano*. 2022;16(11):18579–18591. doi:10.1021/acsnano.2c07027
37. Kumar A, Ali A, Kanika A, et al. Highly Biocompatible Smart Injectable Hydrogel for the Management of Rheumatoid Arthritis. *ACS Biomater. Sci. Eng.* 2023;9(9):5312–5321. doi:10.1021/acsbiomaterials.3c00514
38. Kenechukwu FC, Nnamani DO, Duhu JC, et al. Potential enhancement of metformin hydrochloride in solidified reverse micellar solution-based PEGylated lipid nanoparticles targeting therapeutic efficacy in diabetes treatment. *Heliyon*. 2022;8(3):e09099. doi:10.1016/j.heliyon.2022.e09099
39. Cesur S, Cam ME, Sayın FS, et al. Metformin-Loaded Polymer-Based Microbubbles/Nanoparticles Generated for the Treatment of Type 2 Diabetes Mellitus. *Langmuir*. 2022;38(17):5040–5051. doi:10.1021/acs.langmuir.1c00587
40. Egwuagu CE. STAT3 in CD4+ T helper cell differentiation and inflammatory diseases. *Cytokine*. 2009;47(3):149–156. doi:10.1016/j.cyto.2009.07.003
41. Lindahl H, Olsson T. Interleukin-22 Influences the Th1/Th17 Axis. *Front Immunol*. 2021;12:618110. doi:10.3389/fimmu.2021.618110
42. Makadia HK, Siegel SJ. Poly Lactic-co-Glycolic Acid (PLGA) as Biodegradable Controlled Drug Delivery Carrier. *Polymers (Basel)*. 2011;3(3):1377–1397. doi:10.3390/polym3031377
43. Bouriche S, Cózar-Bernal MJ, Rezgui F, Rabasco Álvarez AM, González-Rodríguez ML. Optimization of preparation method by W/O/W emulsion for entrapping metformin hydrochloride into poly (lactic acid) microparticles using Box-Behnken design. *J Drug Delivery Sci Technol*. 2019;51:419–429. doi:10.1016/j.jddst.2019.03.011
44. Alshehri S, Imam SS. Formulation and evaluation of butenafine loaded PLGA-nanoparticulate laden chitosan nano gel. *Drug Deliv*. 2021;28(1):2348–2360. doi:10.1080/10717544.2021.1995078
45. Brand DD, Latham KA, Rosloniec EF. Collagen-induced arthritis. *Nat Protoc*. 2007;2(5):1269–1275. doi:10.1038/nprot.2007.173
46. Das V, Kroin JS, Moric M, McCarthy RJ, Buvanendran A. Early Treatment With Metformin in a Mice Model of Complex Regional Pain Syndrome Reduces Pain and Edema. *Anesth Analg*. 2020;130(2):525–534. doi:10.1213/ane.0000000000004057
47. Kaplanian M, Philippe C, Eid SA, et al. Deciphering metformin action in obese mice: a critical re-evaluation of established protocols. *Metabolism*. 2022;128:154956. doi:10.1016/j.metabol.2021.154956
48. Dange YD, Honmane SM, Bhinge SD, Salunkhe VR, Jadge DR. Development and validation of UV-spectrophotometric method for estimation of metformin in bulk and tablet dosage form. *INDIAN J PHARM EDUC RES*. 2017;51(4S):S754–S760.
49. Vincy A, Bhatia N, Vankayala R. Optical Characteristics of Indocyanine Green J-Aggregates Induced by Cisplatin for Phototheranostic Applications. *ACS Biomater. Sci. Eng.* 2022;8(12):5119–5128. doi:10.1021/acsbiomaterials.2c01135
50. Wang X, Cao W, Sun C, Wang Y, Wang M, Wu J. Development of pH-sensitive dextran-based methotrexate nanodrug for rheumatoid arthritis therapy through inhibition of JAK-STAT pathways. *Int J Pharm*. 2022;622:121874. doi:10.1016/j.ijpharm.2022.121874
51. Park JY, Kwon S, Kim SH, Kang YJ, Khang D. Triamcinolone-Gold Nanoparticles Repolarize Synoviocytes and Macrophages in an Inflamed Synovium. *ACS Appl Mater Interfaces*. 2020;12(35):38936–38949. doi:10.1021/acsami.0c09842
52. Arlauckas SP, Garren SB, Garris CS, et al. Arg1 expression defines immunosuppressive subsets of tumor-associated macrophages. *Theranostics*. 2018;8(21):5842–5854. doi:10.7150/thno.26888
53. Dowling RJ, Lam S, Bassi C, et al. Metformin pharmacokinetics in mouse tumors: implications for human therapy. *Cell Metab*. 2016;23(4):567–568.
54. Ansari MM, Ahmad A, Kumar A, et al. Aminocellulose-grafted-polycaprolactone coated gelatin nanoparticles alleviate inflammation in rheumatoid arthritis: a combinational therapeutic approach. *Carbohydr. Polym.* 2021;258:117600. doi:10.1016/j.carbpol.2020.117600
55. Ansari MM, Ahmad A, Mishra RK, Raza SS, Khan R. Zinc Gluconate-Loaded Chitosan Nanoparticles Reduce Severity of Collagen-Induced Arthritis in Wistar Rats. *ACS Biomater. Sci. Eng.* 2019;5(7):3380–3397. doi:10.1021/acsbiomaterials.9b00427
56. Pereira A, Brito G, Lima M, et al. Metformin Hydrochloride-Loaded PLGA Nanoparticle in Periodontal Disease Experimental Model Using Diabetic Rats. *Int J Mol Sci*. 2018;19(11):3488.
57. Zhang JM, An J. Cytokines, inflammation, and pain. *Int Anesthesiol Clin*. 2007;45(2):27–37. doi:10.1097/AIA.0b013e318034194e
58. Fukui S, Iwamoto N, Takatani A, et al. M1 and M2 Monocytes in Rheumatoid Arthritis: a Contribution of Imbalance of M1/M2 Monocytes to Osteoclastogenesis. *Front Immunol*. 2017;8:1958. doi:10.3389/fimmu.2017.01958
59. Üçeyler N, Valenza R, Stock M, Schedel R, Sprotte G, Sommer C. Reduced levels of antiinflammatory cytokines in patients with chronic widespread pain. *Arthritis Rheumatism*. 2006;54(8):2656–2664.
60. Hashimoto M. Th17 in Animal Models of Rheumatoid Arthritis. *J Clin Med*. 2017;6(7):73.
61. Denton ML, Foltz MS, Estlack LE, et al. Damage thresholds for exposure to NIR and blue lasers in an in vitro RPE cell system. *Investigative Ophthalmol Visual Sci*. 2006;47(7):3065–3073.
62. Fresneda Alarcon M, McLaren Z, Wright HL. Neutrophils in the Pathogenesis of Rheumatoid Arthritis and Systemic Lupus Erythematosus: same Foe Different M.O. *Front Immunol*. 2021;12:649693. doi:10.3389/fimmu.2021.649693
63. Li S, Yin H, Zhang K, et al. Effector T helper cell populations are elevated in the bone marrow of rheumatoid arthritis patients and correlate with disease severity. *Sci Rep*. 2017;7(1):4776. doi:10.1038/s41598-017-05014-8
64. Baggiolini M, Dahinden CA. CC chemokines in allergic inflammation. *Immunol Today*. 1994;15(3):127–133.
65. Langs G, Peloschek P, Bischof H, Kainberger F. Automatic quantification of joint space narrowing and erosions in rheumatoid arthritis. *IEEE Transactions Med Imaging*. 2008;28(1):151–164.